Unique properties and behavior of non-mercerized type-II cellulose nanocrystals as carbon nanotube biocompatible dispersants

Jose M González-Domínguez,[1] Alejandro Ansón-Casaos,[1] Laura Grasa,[2,3,4] Luis Abenia,[1‡] Alba Salvador,[1‡] Eduardo Colom,[1] Jose E. Mesonero,[2,3,4] J. Enrique García-Bordejé,[1] Ana M. Benito,[1] Wolfgang K. Maser.[1]*

AUTHOR ADDRESSES: 1) Group of Carbon Nanostructures and Nanotechnology, Instituto de Carboquímica ICB-CSIC. C/ Miguel Luesma Castán 4, 50018 Zaragoza (Spain); 2) Departamento de Farmacología y Fisiología, Facultad de Veterinaria, Universidad de Zaragoza, C/ Miguel Servet s/n, 50013, Zaragoza (Spain); 3) Instituto de Investigación Sanitaria de Aragón (IIS Aragón); 4) Instituto Agroalimentario de Aragón (IA2).

KEYWORDS: nanocellulose, acid hydrolysis, allomorphs, carbon nanotubes, dispersion, biocompatibility, human intestine.

ABSTRACT: Nanocellulose is increasingly being investigated as a paradigm of a sustainable nanomaterial, because of its extraordinary physical and chemical properties, together with its renewable nature and worldwide abundance. The rich structural diversity in cellulose materials is represented by different crystalline allomorphs, from which types I and II stand out. While type I is naturally and ubiquitously

present, type-II is manmade and requires harsh and caustic synthesis conditions such as the so-called mercerization process. Here we provide an optimal scenario to obtain either type-I or II nanocrystalline cellulose (NCC) by a mercerization-free method consisting only on the acid hydrolysis commonly used to produce nanocellulose from microcellulose. The possibility of having non-mercerized type-II NCC acquires a great relevance, since this nanostructure shows particularly appealing properties. Moreover, an entangled and wrapped system arises when used as a dispersing agent for single-walled carbon nanotubes (SWCNTs), significantly different from that of type-I. The biological testing of each NCC type and their respective SWCNT-NCC dispersions in human intestinal (Caco-2) cells reveals a general innocuous behavior, in both cancer and normal stages of differentiation, however the type-II based SWCNT-NCC dispersions display cytotoxicity for cancer cells, while enhancing mitochondrial metabolism of normal cells.

INTRODUCTION

Nanotechnology is heading towards more and more sustainable and 'green' principles, based on renewable sources, and preferably compatible with aqueous media. Over this horizon, novel nanostructures and nanocomposites, fulfilling these standards have emerged, with an emphasis on natural origins (polypeptides, polysaccharides…), biocompatibility and degradability.[1] Cellulose is the most abundant biopolymer on Earth, and its availability, renewability and hydrophilic character (stemming from its rich hydroxyl-based surface composition) have sparked its study at the nanoscale in the form of nanofibrils or nanocrystals.[2] As for the latter ones, these are produced via top-down approaches based on the acid hydrolysis of lignocellulosic biomass, in order to selectively hydrolyze the amorphous phase and isolate the nanometric crystalline domains within its structure. The resulting nanocrystalline cellulose (NCC) has needle-like or rod-like morphology with dimensions of 3-10 nm diameter, an aspect ratio higher than 5, and outstanding properties:[3] For example, high tensile strength (~7500 MPa), mechanical moduli up to 130-140 GPa, high surface area (~250 m^2/g), generally accepted biocompatibility, and a huge versatility in surface functionalization.[4,5] These will warrant a promising future in the development of multifunctional materials, sensors

and structures, with the same success as previous nanostructures, but with better prospects of sustainability and cost-effectiveness.[6]

From a structural point of view, cellulose chains have a directionality at a macromolecular level,[7] defining the type of crystal structure upon the relative disposition of such chains. There are up to four described crystalline types of cellulose (from I to IV), being I and II the most reported and studied. The most common crystalline polymorph (a.k.a. allomorph) is the so-called type-I, which is dominant in natural cellulose sources, exhibiting a parallel arrangement of chains.[8] Besides, type-I may exist in two different forms, namely I_α and I_β, which only differ in their kind of unit cell. Type-I_α is a meta-stable phase with a triclinic unit cell provided of one cellulose chain, while type-I_β has a monoclinic unit cell with two chains. Type-II cellulose allomorph, in turn, displays polymeric chains in antiparallel fashion. Despite type-II being the most thermodynamically favored cellulose allomorph, its presence in natural sources is negligible and the way of obtaining it is by chemical transformation from type-I in an irreversible manner.[8,9] On the one hand, the dissolution and recrystallization of type-I cellulose yields the type-II (a material known as regenerated cellulose), and this needs specific chemicals such as ionic liquids[10,11] and/or organic solvents.[12,13] On the other hand, and perhaps the most extended method to turn type-I cellulose into type-II, is the soaking in concentrated NaOH solutions (typically around 15-20 wt%), a process named mercerization, and known since the mid-19th Century.[3,7,8,9] It is widely accepted that the solid-state reaction taking place between NaOH and type-I cellulose starts by a swelling of cellulose crystals, breaking the existing hydrogen bonds,[9] followed by a chain intermingling that causes a reconfiguration of these bonds towards the antiparallel fashion.[7,8]

The mercerization strategy could raise environmental concerns, as for the harsh and caustic substances employed, whose remnants might also pose unforeseen hazards if the fate of such type-II NCC is envisioned in biological or biomedical applications. Nevertheless, there is a landmark work showing the possibility of obtaining type-II NCC without mercerization.[14] This report, from 2012 by Sèbe et al., clearly demonstrated the feasibility of obtaining type-II NCC by only sulfuric acid treatment, without the need

of any alkaline treatment to the feedstock.[14] This striking discovery meant that mercerization can be circumvented, and thus type-II NCC can be obtained in the course of acid hydrolysis, saving time, costs, and entailing a somewhat more environmentally friendly scheme. However, surprisingly and to the best of our knowledge, this method has gone largely unnoticed thereafter, in favor of mercerization, until just very recently a few authors have started to apply it again.[15,16]

Despite being widely reported in the literature for the last decade, type-II cellulose nanocrystals have been highly disregarded in terms of potential applications, as the majority of scientific studies only focus in their preparation and characterization.[8,9,17,18] NCC types I and II do not only differ in their crystalline structure and morphology, but also in their properties and behavior. From the very scarce studies that paid attention to this fact, it is known that in Pickering emulsions, the emulsion ratio is higher and droplet sizes are smaller when made upon type-I NCC in comparison to type-II.[19] This would open a venue to tune oil-in-water emulsions by only choosing a specific NCC type. Another difference is that type-II NCC seems to be more enzymatically degradable than type-I,[20,21,22] so the former one would be a much more convenient candidate to conform fully biodegradable materials or structures. Hence, there is still great room to unravel and exploit NCC through the study of its type-II and application in many fields.

One possible venue would be the combination of NCC with other carbon nanostructures. While hybrid nanomaterials between two different carbon nanostructures are widely reported in literature,[23,24] those composed of NCC and carbon nanostructures are certainly rare. Practically all these limited examples consist of a simple mixing of components, mostly without accomplishing the synergistic characteristics of a hybrid. Moreover, a recurrent strategy is to induce an aqueous affinity to the system by providing either oxidized carbon nanostructures (e.g. graphene oxide),[25] or oxidized/carboxylated NCC,[26] so the hybrid materials born thereof exhibit aqueous processability,[27,28] usually at the expense of mechanical and electrical properties. There is only one precedent that unambiguously addresses the achievement of a hybrid nanomaterial composed of unmodified carbon nanotubes (CNTs) and unmodified NCC, reported by Chauvet and co-workers.[29] It was demonstrated that non-oxidized CNTs (either single-walled or multi-

walled) can be efficiently dispersed in an unmodified NCC aqueous colloid, resulting in a very stable hybrid material in water. However, no reports have been found on the use of type-II NCC for this purpose, or the potential of NCC for dispersing other kinds of non-oxidized CNTs. It is well known that a traditional bottleneck for the development of carbon nanotubes or graphene materials is their proper processability in water, requiring harsh chemical treatments or the use of large amounts of toxic surfactants or organic solvents,[30] so the use of NCC could provide a friendlier approach for the aqueous processing of non-oxidized hydrophobic carbon nanostructures.

In the present work, we have performed a systematic parametric study to selectively synthesize type-I or type-II NCC by only making use of chemical hydrolysis with sulfuric acid. The preparation procedure has been optimized to provide the basis to achieve a tailored outcome, ranging from nearly pure NCC crystalline types (I or II) to customized mixtures of both. Furthermore, the implications of interfacing one type of NCC or another with carbon nanotubes provides surprising results in the NCC behavior as dispersing agents and in the biocompatibility and bioactivity of the resulting dispersions.

EXPERIMENTAL SECTION

Materials and reagents. The cellulose source employed in this work was a microcrystalline cellulose (MCC) in powder from cotton linters with 20 μm average particle size (Sigma Aldrich, ref. 310697). Sulfuric acid (98%) was acquired from Labkem (Barcelona, Spain). Any use of water reported here corresponds to ultrapure water, obtained from a Siemens Ultraclear device, whose water has a conductivity of 0.055 μS/cm. Single-walled carbon nanotubes (SWCNTs), produced by the electric arc discharge method, were purchased form Carbon Solutions Inc. (California, USA) in pristine form (AP grade). These SWCNTs were purified in-house by a combination of oven treatment (350ºC, 2h) and HCl reflux (3M, 2h), as reported elsewhere.[31]

Synthesis of NCC: All experiments were carried out starting from 10g of MCC. This was placed in a 500 mL round-bottom flask; 45 mL of ultrapure water were poured onto it and the blend was bath-sonicated (45 kHz) during 10 min for homogenization. The flask was placed in an ice/water bath at 0ºC and magnetically stirred until the temperature of the medium was stabilized. Then, another 45 mL of H_2SO_4 (98%) was slowly added, dropwise, always with constant magnetic stirring. The dripping rate is recommended at 1 droplet for every ~5s. Special care must be taken to sustain the stirring, since the reaction medium progressively becomes more and more viscous, and a defective homogenization will result in a deviation from the expected outcome, or even the burning of the sample. Once the acid dripping finishes, the final sulfuric concentration in the reaction medium reaches 64 wt%. In those experiments where 50 wt% H_2SO_4 is intended, another 33 mL of water were dropwise added right after the sulfuric acid dripping finishes, again at 0ºC and with constant magnetic stirring. It is important to note that using a 50wt% H_2SO_4 solution from the beginning of the process does not provide the same results, as the contact with concentrated acid is necessary to favor cellulose swelling (see below). Immediately after the last droplet is added, the flask is brought to a heating plate and treated at a specific temperature for a given time (see Scheme 1), always with constant stirring. Then, the medium is poured on a 10-fold excess of cold water and left to settle down overnight in a fridge at 4ºC. The sedimented solid was partly separated from the liquid by slow decanting, and this process was repeated once more. The remaining suspension was inserted into a dialysis sack (SpectraPor®1, Spectrum Labs, regenerated cellulose, 6-8 kDa molecular weight cutoff) and dialyzed against water inside a 5L beaker, with frequent water replacements, until no acid is detected in the dialysis waters. The dialyzed suspension was separated in 45 mL sized aliquots, centrifuged at 16000 rcf for 1 min, and the supernatant liquid decanted off. The pellets were redispersed in 45 mL of water each, and centrifuged again in equal conditions. The centrifugation was stopped once the supernatant liquids showed no appreciable amount of NCC in suspension. The whole amount of accumulated NCC water colloid was stored in a fresh place and kept away of sunlight. Unless otherwise stated, NCC was employed in the form of such aqueous colloid; only in specific characterization techniques, a lyophilized

fine powder (Telstar Cryodos freeze drier, -49ºC, 0.3 mbar) was employed. Besides, by means of the freeze drying technique, the mass concentration of the as-prepared NCC colloids (in mg/mL) could be obtained, as well as the mass yield of the whole hydrolysis process, taking into account the starting 10mg of MCC. In average, NCC aqueous colloids were obtained in the range of 2-3 mg/mL, and the full conversion yield from MCC to NCC in the range of 10-20 wt%.

SWCNTs dispersions in NCC: In a typical experiment, 10mg of SWCNTs were put in touch with 10mL of an as-produced NCC aqueous colloid (3 mg/mL), either type-I or II. The system was sonicated with a sonic tip (Hielscher DRH-P400S; 400 W maximum power; 24 kHz maximum frequency at 60% amplitude and 50% cycle time) for 1h while externally cooled with an ice/water bath. The resulting dispersion was left to settle down overnight, the supernatant liquid was carefully decanted and subjected to ultracentrifugation (Beckman Coulter L-100 XP ultracentrifuge, SW55Ti rotor, Beckman tubes ref. 326819) at 120000 rcf for 1h. After this process, the supernatant liquid was again carefully extracted, and the remaining pellet was discarded. All subsequent characterizations and biological tests to SWCNTs dispersions were performed on these latter supernatants, which were determined to have a concentration of SWCNTs of about 0.1 mg/mL.

Characterization techniques: X-Ray diffraction (XRD) patterns were collected with a Bruker D8 Advance diffractometer using a Cu tube as the X-ray source (λ Cu Kα = 1.54 Å), a tube voltage of 40 kV, and a current of 40 mA. The results were recorded in Bragg−Brentano geometry in the range of 2θ = [5°−40°], with steps of 0.05° and 3s accumulation time. Samples were measured in powder state and analyzed with the fitting software Topas 5.0.

Thermogravimetric analysis (TGA) was carried out in a Netzsch TG 209F1 device, in nitrogen atmosphere (60 mL/min) and a heating rate of 10ºC/min, to sample aliquots (solid fine powder) of about 10mg, exactly weighed. Each represented plot is the average of several recordings.

FTIR spectra were acquired using a Bruker Vertex 70 spectrophotometer. Lyophilized NCC samples were milled in agate mortar with spectroscopic-grade KBr, and the resulting pellet was recorded in the

400-4000 cm^{-1} range in transmittance mode. SWCNT dispersions were measured in the NIR region in a liquids cell, with a previous dilution in ultrapure water in order to reach an absorbance value of ~0.4 at 850nm.[32] The same diluted sample was also measured in the UV-Vis region by means of a Shimadzu UV-2401PC spectrophotometer. Both NIR and UV-Vis spectra are herein represented in a single plot for the sake of clarity. Since SWCNT concentration is directly proportional to the sample absorbance (optical thickness), ultra-centrifugation yields (in mass%) were calculated as the ratio of the respective absorbances (before and after ultracentrifugation) at 850 nm. [32] NIR purity indexes were calculated through the S_{22} van Hove transition, as the ratio between the peak area and the full spectral area in this particular region.[32]

Particle size and Zeta potential were measured directly to aqueous colloids in a Malvern Nano ZS instrument, according to the principles of dynamic light scattering (DLS) and electrophoresis, respectively. The device measures the particle size distribution through the DLS approach by irradiating with a He−Ne laser at 633 nm, and applying the Stokes-Einstein equation while assuming a single and constant diffusion rate (i.e. spherical particles). The Zeta value was internally calculated from the electrophoretic mobility using Henry's equation. In the case of SWCNTs dispersions, supernatants were measured after diluting them as described earlier for absorption spectroscopies. For the DLS measurements, a refractive index of 1.47 was taken for cellulose species, while 2.42 (carbon) was taken for SWCNTs. Measurements were carried out in disposable polystyrene dip cells (code DTS1061). All Zeta potential measurements were performed at least by triplicate, and are referred to an average pH of 4.6 (NCC aqueous colloids) or 5.2 (SWCNTs aqueous dispersions) and a room temperature of 25ºC.

Transmission electron microscopy (TEM) images were obtained with a JEOL-200FXII microscope. Samples were prepared by drop casting liquid samples onto carbon-coated, 400-mesh copper grids (Electron Microscopy Sciences, Ref. CF-400CU).

Cell culture: This study was carried out in the human enterocyte-like cell line Caco-2/TC7,[33] kindly provided by Dr. Edith Brot-Laroche (INSERM, UMR S 872, Centre de Recherches de Cordeliers, Paris,

France). This cell line undergoes in culture a process of spontaneous differentiation that leads to the formation of a monolayer of cells, expressing morphological and functional characteristics of the mature enterocytes. This differentiation process is growth-dependent, where the cells undergo differentiation from 'undifferentiated proliferative crypt-type cells' in exponential phase of growth, to 'differentiated enterocyte-type cells' in stationary phase.[34] Caco-2/TC7 cells (passages 30-50) were cultured at 37ºC in an atmosphere of 5% CO_2 and maintained in high glucose DMEM supplemented with 2 mM glutamine, 100 U/mL penicillin, 100 µg/mL streptomycin, 1% non-essential amino acids, and 20% heat-inactivated fetal bovine serum (FBS) (Life Technologies). To cell line maintenance, cells were passaged enzymatically with 0.25% trypsin-1 mM EDTA and sub-cultured on 25 cm^2 plastic flasks at a density of 10^4 cells/cm^2. Culture medium was replaced every 2 days. With this density of culture, the cells reach cell confluence 90 % (where cell differentiation starts) at 7 days after seeding, and the complete cell differentiation is reached at 15 days post-seeding. Thus, experiments in undifferentiated and differentiated cells (considered as cancer and normal cells, respectively) were performed between 2-5 days and 12-15 days post-seeding, respectively. Cells were seeded in 96-well plates at a density of 2×10^4 or 4×10^3 cells per well, and measurements were carried out 5 or 15 days after seeding, respectively. The culture medium was replaced with fresh medium (without FBS) containing the samples at the required concentrations varying from 0 to 5 ng μl^{-1}, and with an exposure time of 72 h.

Cell viability assay: Cell survival was measured by using the MTT test. The assay is dependent on the cellular reduction of 3-(4,5-dimethylthiazol-2-yl)-2,5-diphenyltetrazolium bromide (MTT, Sigma) by the mitochondrial dehydrogenase of viable cells to a blue formazan product that can be measured spectrophotometrically. Following the appropriate incubation of cells, with or without the samples, MTT (5 mg mL^{-1}) was added to each well in an amount equal to 10 % of the culture volume. Cells were incubated with MTT at 37 °C for 3 h. After that, the medium and MTT were removed and 100 µl of DMSO was added to each well. The plate was gentle stirred in a shaker. Finally, the cell viability was determined by measuring the absorbance with a multi-well spectrophotometer (DTX 800 Multimode Detector, Beckman

Coulter) at a wavelength of 560 nm and compared with the values of control cells incubated in the absence of the samples. Experiments were conducted in triplicate wells and repeated at least three times.

RESULTS AND DISCUSSION

General overview. Types I and II cellulose nanocrystals have been produced by a mercerization-free process, in essence, treating a cellulose source with acid hydrolysis. H_2SO_4 is a feasible swelling agent of cellulose but it is also highly reactive,[35,36] being imperative that such swelling is favored against hydrolysis (depolymerization) to obtain type-II NCC, and vice versa for type-I. There is a certain range of temperature and concentration conditions in which H_2SO_4 behaves more as a hydrolytic or swelling agent, respectively.[35,36] Thus, we have taken this into account when exploring the circumstances in which it is possible to control swelling against hydrolysis. **Scheme 1** displays a general overview of the experimental variables studied. Sèbe and co-workers,[14] postulated that obtaining type-I or II NCC was sensitive to the H_2SO_4 amount and addition time. Here we demonstrate that such control over the crystalline allomorph can be exerted *via* the acid concentration, treatment time and temperature. One important first consideration is the acid addition rate over the initial MCC suspension. A rapid addition of the acid will boost the hydrolysis pathway, by creating locally high acid-to-cellulose ratios (kinetic control), resulting in the maintenance of the preceding type-I allomorph. In turn, an excessively lengthy addition will result also in hydrolysis again by kinetic reasons. Only an intermediate contact time between cellulose and H_2SO_4 seems to be the optimum to end up in type-II allomorph, by maximizing the swelling effect (responsible for the hydrogen bond breakage and chain intermingling[9]) while keeping hydrolysis to a minimum extent during the addition step. Similarly, Sèbe et al.[14] reported the most prominent type-II XRD features at intermediate acid addition rates. Here we hypothesize that this control over the NCC crystalline type is actually dependent on the acid exposure conditions (contact time and temperature) at a given H_2SO_4 concentration. In order to suppress parasitic external influences, we have kept a steady acid addition rate (1

droplet at every ~5s) and a constant and vigorous magnetic stirring along the whole synthetic procedure. We have explored two different H_2SO_4 concentrations, namely 64wt% and 50wt%. The former one is a widely reported benchmark, while the latter is the lowest found published in this context.[7,16] The great majority (if not all) of NCC syntheses are carried out between these two H_2SO_4 concentration values, so all of our experiments have focused these two limiting values. An important detail is that all treatments with 50 wt% H_2SO_4 have been carried out by further dilution of the 64 wt% case, i.e. dripping a volume of water right after the acid dripping had finished. In this way, we intended to boost the swelling effect of concentrated H_2SO_4.

In general terms (**Scheme 1**), we find out that 64 wt% H_2SO_4 is able to produce exclusively type-I NCC at high treatment temperatures (70ºC) but in short reaction times (10 min). Longer times will result in fail, as the sample will burn, but this won't happen if 50 wt% H_2SO_4 is used. In this case, treatments up to 40 min will provide an essentially type-I NCC, but with an appreciable amount of type-II (named as type-I + II). In order to increase the ratio of type-II in the NCC sample, a combination of 64 wt% H_2SO_4, lower treatment temperatures and longer times is necessary (named as type-II + I), until reaching an exclusively type-II NCC at room temperature (27ºC) and a relatively long treatment time (5h). In-between conditions would lead to intermediate outcomes. In this whole scenario, the inferred insights point to the fact that there is a delicate equilibrium between hydrolysis and swelling. Concentrated H_2SO_4 (64 wt%) seems necessary for type-II NCC to be reached, as this concentration provokes the swelling of cellulose crystalline domains (if enough time is given) thus leading to the thermodynamically favored antiparallel chain rearrangement. But for this to happen, the hydrolysis rate needs to be slowed down as much as possible, mainly by using low treatment temperatures. By using more aggressive conditions (i.e. higher treatment temperatures), hydrolysis is boosted and swelling cannot take place in time, so the eventual NCC retains the original type-I crystallinity. These guidelines are intended to serve as a roadmap to predict the allomorph type or ratio by choosing the proper experimental combination, with the added advantage of avoiding alkaline treatments or re-crystallization procedures.

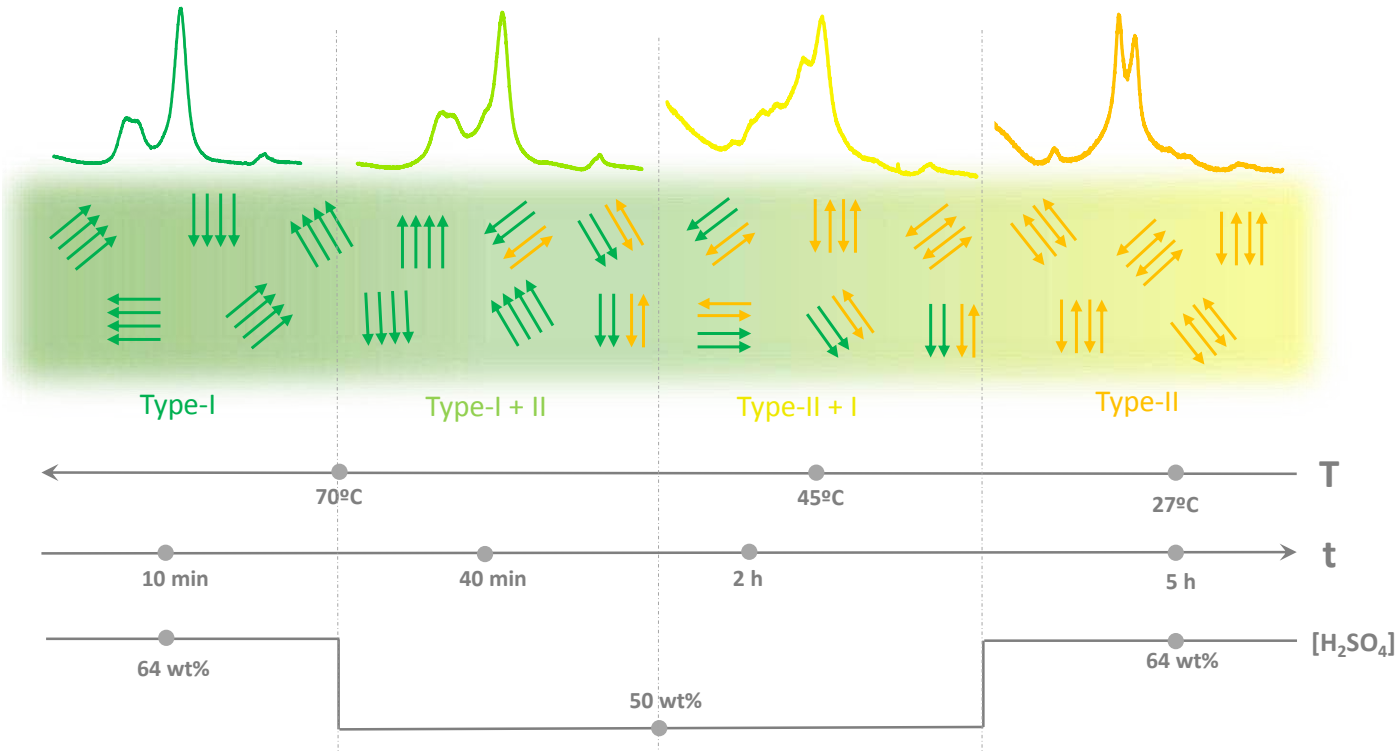

Scheme 1.- Representation of the different experimental conditions to obtain NCC type-I (green), type-II (orange) or their mixtures. Arrows represent the cellulose chain orientation within nano-crystals. The upper graphs correspond to representative X-Ray diffractograms in the range of 2θ = 5º-40º. The bottom lines indicate the process variables. Temperature (T) and time (t) follow inverse trends, while sulfuric acid concentration ([H_2SO_4]) affects differently being 50wt% or 64wt%. Vertical dotted lines provide visual aid.

Evaluation of crystalline structures. In order to verify the successful achievement of different NCC allomorphs and mixtures, we rely on the XRD technique.[37,38] We analyzed many different diffractograms for each situation described in **Scheme 1**, and a representative profile in each case is shown in **Figure 1**, together with the MCC for comparison. We have also analyzed in depth their diffractograms by signal deconvolution (**Figure 1**, **Table 1**). The starting MCC has a clear type-I profile, provided of three main peaks at 2θ = 22.5º (200), 16.6º (110) and 14.9º (1-10), which is perfectly consistent with other works for this particular biomass source.[39,40] Besides, there is a shoulder at 2θ = 20.9º (102) which also appears in type-I celluloses,[39] although it is not observed by all authors. In those experimental conditions leading to

NCC with a main type-I character, these features are kept as such, except for the (102) shoulder, which seems to disappear in the most efficient hydrolysis conditions[39] (Table 1), suggesting that this crystalline plane is more reactive and sensitive to hydrolysis than the other ones for type-I profiles. In the type-I + II mixture, the (102) shoulder is present, but at a slightly lower diffraction angle, which might be related to the existence of a type-II component nearby (see below). Besides, the (200) component is slightly up-shifted for type-I NCC as compared to that of MCC. In predominantly type-II NCC samples, new XRD features arise as a consequence of their different crystalline structure. On the one hand, a characteristic peak appears at nearly $2\theta = 12.4^{\circ}$, corresponding to their own (1-10) diffraction plane.[8,14,16,17] Furthermore, the contributions named as peak 4 and peak 5 (**Table 1**) experience a downshift with respect to type-I samples, which entails a different diffraction planes assignment: (110) and (020) respectively, which are also typical from type-II NCC.[8,16,41] In the type-II + I sample, the type-I diffraction peaks from (110) and (1-10) crystalline planes are still visible, but these are almost depleted in the pure type-II sample, pointing to the mixed nature of the former. In general, the progression from type-I to type-II NCC with varying experimental conditions is clearly visible from XRD profiles, leading to different diffraction patterns according to the sample nature (**Scheme 1** and **Figure 1**).

An additional analysis was carried out by quantifying the peak areas under the aforementioned components (**Figure S1**, Supporting Information). Thus, we estimate that upon acid hydrolysis of MCC we are able to reach NCC in the range from ~90% type-I (and the rest assumed as amorphous cellulose) to ~90% type-II (and the rest assumed as type-I cellulose), plus intermediate situations depending on the experimental variables.

Colloidal stability, size and morphology of NCC. It is known that the sulfuric acid hydrolysis entails a concomitant insertion of a certain (random) number of sulfate ester groups, grafted to some native –OHs.[4] This fact completely changes the chemical nature of the as-prepared NCC, by providing a negatively charged surface and entailing a noticeable water dispersibility. Our freshly prepared aqueous NCC colloids were evaluated by DLS and electrophoresis in order to acquire insights into their size and stability.

Figure 2 shows a data summary of such results, classified by the NCC allomorph kinds. The herein reported size, is ascribed to an "apparent (or equivalent) particle size", in terms of hydrodynamic diameter, but not actually representing the NCC dimensions, as nanocrystals have a high aspect ratio with complex and varying diffusion constants which strongly deviate from an ideal spherical shape. Nevertheless, DLS can be consistently used as a reference method to compare the state and quality of a dispersion in cases such as this, where a series of samples is analyzed with identical sample preparation and measurement protocols.[42] The diameters found for our NCC samples (**Figure 2**, bars), show that type-II NCC is more than double the apparent size of type-I, and the mixed allomorphs samples correlate with intermediate values. This could be attributed to a much stronger hydrophilic character of type-II NCC, compared to type-I. In fact, this has been recently pointed out by some authors,[19] who found a significantly lower contact angle (H_2O) and higher surface energies for type-II NCC than for type-I. This would cause type-II NCC to interact in a higher extent with the surrounding water molecules, increasing their hydrodynamic size. In turn, Zeta potential value is directly proportional to such stability. In our samples, all values are negative in sign, and are above 20 mV in absolute value, which is the generally accepted threshold of stability. There were no significant differences among all the samples, which exhibited Zeta potentials in the range of -30 to -40 mV, in perfect agreement with common literature values.[42]

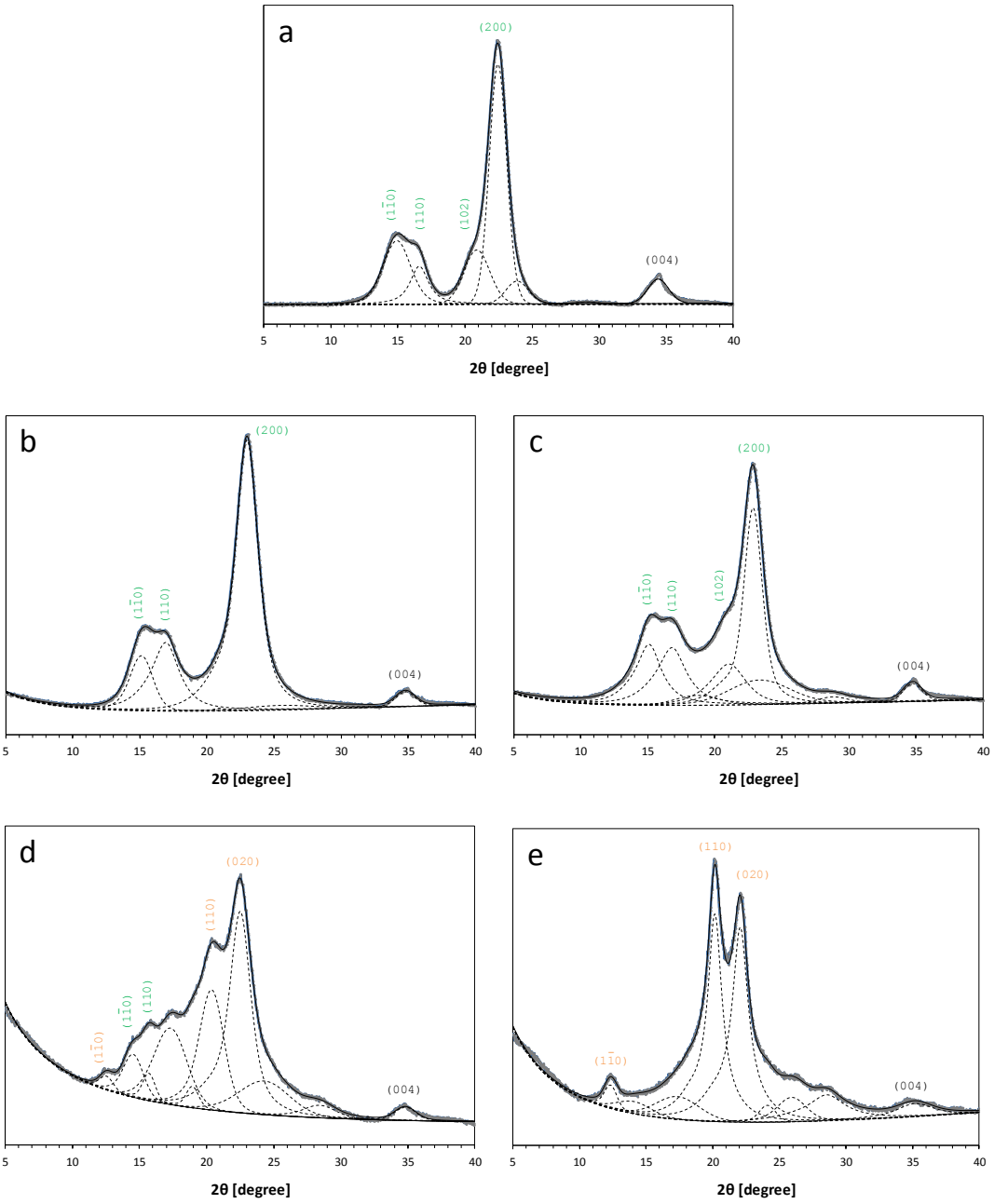

Figure 1.- XRD patters for different cellulose samples. (a) MCC; (b) Type-I NCC; (c) Type-I + II NCC; (d) Type-II + I NCC; (e) Type-II NCC. Miller indexes of the main crystalline planes are displayed either in green or orange, in order to account for their correspondence with Type-I or II allomorph respectively.

Table 1. XRD peak positions (2θ, in degrees) for the different deconvoluted signals from Figure 1. Peaks are arbitrarily numbered following an increasing order of diffraction angle, and assigned to their corresponding crystalline planes in type-I or II allomorphs.

	Peak 1 (1-10)-II	Peak 2 (1-10)-I	Peak 3 (110)-I	Peak 4 (102)-I (110)-II	Peak 5 (200)-I (020)-II
MCC		14.9	16.6	20.9	22.5
NCC Type-I		15.0 ± 0.1	16.8 ± 0.1		22.8 ± 0.1
NCC, Type-I + II		15.0 ± 0.1	16.8 ± 0.1	20.6 ± 0.7	22.8 ± 0.1
NCC, Type-II + I	12.5 ± 0.3	14.5 ± 0.2	15.9 ± 0.5	20.4 ± 0.1	22.5 ± 0.1
NCC, Type-II	12.4 ± 0.1	14.8 ± 0.2	16.8 ± 0.2	20.2 ± 0.1	22.3 ± 0.2

The dimensions, shape and morphology of the different NCC allomorphs were corroborated by TEM. **Figure 3** shows some microscopic images taken for type-I and II NCC respectively. It is worth recalling that TEM and DLS provide complementary information, since the former shows the actual sizes and morphologies while the latter is a measure of the nanoparticle + solvation sphere set. Our TEM observations are consistent with the current knowledge on NCC: type-I appears as needle-like particles with an average of 200-300 nm length, and 5-10 nm width. Conversely, type-II presents a fully different aspect, more twisted and ribbon-like, with shorter lengths (50-100 nm) and thicker widths (15-20 nm). This difference in morphology has been evidenced in literature, agreeing in the fact that type-II NCC is made of shorter, but wider, particles.[7,8,14,18]

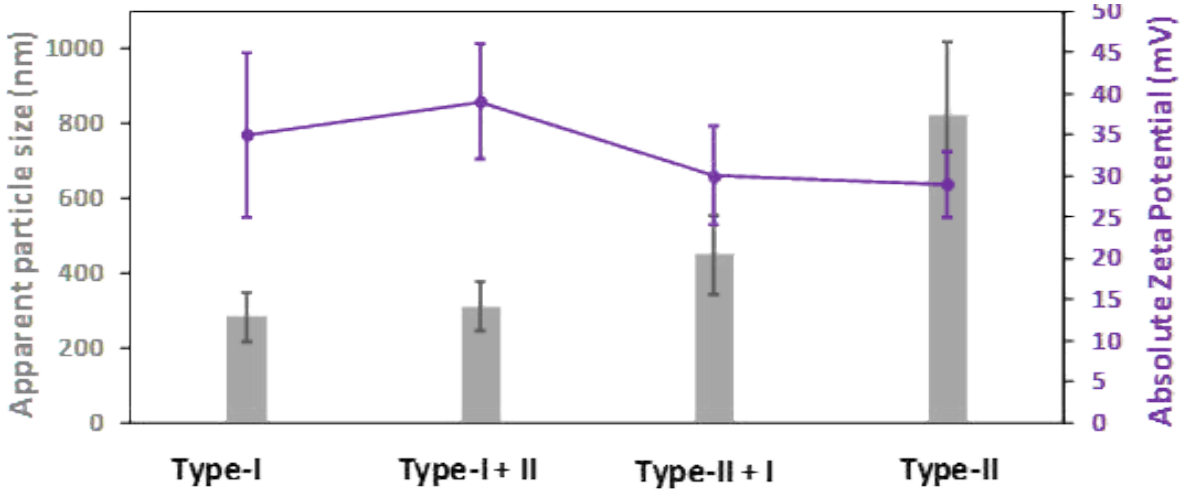

Figure 2.- Apparent particle size (bars) and Zeta potential (point-line) values for the different NCC allomorphs and mixtures, obtained from DLS and electrophoresis, respectively. Size corresponds to hydrodynamic diameter. Error bars correspond to standard deviations from 3-6 repetitions.

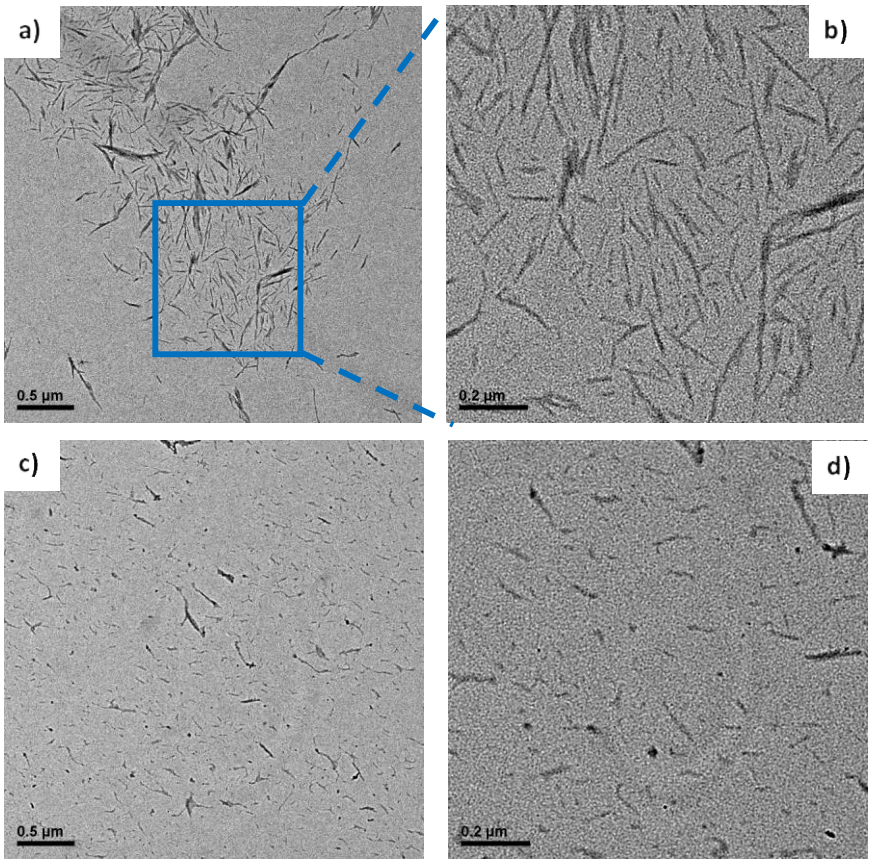

Figure 3.- TEM images for type-I (a,b) and type-II (c,d) NCC samples. Figure 3b corresponds to an inset of Figure 3a.

Chemical nature of NCC. The chemical composition and nature of the as-prepared NCC samples were evaluated through thermal stability and FTIR spectroscopy. **Figure 4a**, displays representative thermograms of the different samples, together with the parent MCC (for precise temperature assignments, differential thermograms, dTGs, are presented in **Figure S2** in Supporting Information). At the earliest stages (temperature range 25-120ºC), all samples exhibit a slight weight loss (≤ 2 wt%) due to their moisture content. The most visible feature is that MCC presents higher thermal stability (later onset and higher maximum degradation rate temperature) than the derived NCC samples, which is usually pointed out elsewhere.[9,39,40,43] These markedly different profiles stand as the first evidence of a successful achievement of NCC from MCC. In fact, there are several proposed reasons why this occurs,[39] including an increased surface area of NCC as compared to MCC, or a more effective heat transfer and thermal conductivity of nanocrystals; but by far the most convergent explanation is the presence of sulfate ester groups (coming from the sulfuric acid hydrolysis),[39,43] which can catalyze the thermal decomposition of the cellulose materials, possibly changing the involved mechanisms, and eventually compromising the overall thermal stability. A sharp single weight loss is observed for MCC, centered at 338ºC and with onset at approximately 260ºC and ascribed to the collapse of the glucosidic structure and aromatization of the sample.[43] All the NCC materials exhibit a multi-step weight loss in the range of 140-300ºC, which are mainly due to the formation of carbonyl compounds and gasification processes.[39,43] A significant feature is that the lower thermal stability (earlier onsets and lower maximum degradation rate temperatures) is associated with the higher type-II character of the NCC, and this fact points towards a higher sulfation degree, see below). Furthermore, the amount of solid residue remaining at 800ºC (which corresponds to the annealed carbonaceous leftovers from the cellulose pyrolysis process) also correlates with the type of NCC allomorph. The higher the type-II content, the more the solid residue remaining in TGA. As a matter of fact, such residue in inert atmosphere TGAs can be related to the flammability of the material, whereby the synthesized type-II allomorphs exhibit enhanced flame resistance.[44] (**Table S1** in **Supporting Information**).

Since thermal stability of NCC is highly sensitive to its surface chemical nature,[40,43] we have attempted to analyze the composition of our NCC samples through FTIR spectroscopy (**Figure 4b**). There are common features to all samples, namely their moisture content, by the bands at ~3400 cm^{-1} and 1635 cm^{-1}, the stretching vibration of C-H bonds at about 2900 cm^{-1}, the antisymmetric vibration of C-O-C glycosidic bonds at 1160 cm^{-1}, or the C-O stretching vibrations at 1032 and 1057 cm^{-1} (C3 and C6 respectively).[17,18,39,42] Besides, we found that both the parent MCC and all type-I allomorphs thereof are type-I_β, as for the O-H stretching and out-of-plane bending which respectively appear at 3270 and 710 cm^{-1}.[39] There are, though, other bands that differ between allomorphs, such as the C-O stretching vibration of C2, which appears in our case at 1113 cm^{-1}. This band is fairly visible in type-I allomorphs, but gets quite depleted when NCC has a high content in type-II. Similarly the band at 1430 cm^{-1}, ascribed to the CH_2-(C6) bending vibration, is also being noticed in mercerized NCC.[18] According to the hydrogen bonding reconfiguration that type-I experiences upon swelling, the C6 of a given chain shifts from a C3 bonding to a C2 bonding to the adjacent chain, ending up in a more cross-linked conformation.[45] This could cause the C-O stretching to be hindered, thus diminishing its corresponding IR band in type-II allomorphs.[18] Another proof of allomorphs difference in FTIR comes from the C-O-C symmetric vibration of β-glycosidic bonds, which appears near 900 cm^{-1}. Our results are coincident with the literature,[18] as we found this band at 898 cm^{-1} for type-I NCC and at 895 cm^{-1} for type-II. Again, the different interchain structure may be a suitable explanation for this fact. Finally, the sulfate ester presence was also spotted in the FTIR spectra; in particular, the asymmetric SO_2 stretching (at 1370 cm^{-1}), common to both allomorphs. Further, the symmetric SO_2 stretching of sulfate esters is only visible (and very prominent) in the purest type-II allomorph, suggesting that this sample contains a higher extent of sulfation (as already hypothesized in previous discussions). In order to confirm this, we performed some elemental analysis (data not shown), and we observed that the sulfur content in predominantly type-I samples was in the range of 0.3-0.8 wt%, while predominantly type-II samples showed a sulfur content of 1-2 wt%.

From TGA and FTIR characterization we demonstrate that the thermal stability and surface chemistry of the different NCC samples correspond to a well-defined and selectively prepared cellulose allomorph (or mixture), being a reliable fingerprint of each case, and mostly coincident with those results obtained by mercerization or regeneration (in the type-II case). However, there are new implications in type-II NCC, as the acid hydrolysis method provides significantly higher amounts of sulfate ester groups grafted to the nanocrystals. This reveals that the resulting material has a unique composition and behavior, further contributing to the much larger hydrodynamic sizes.

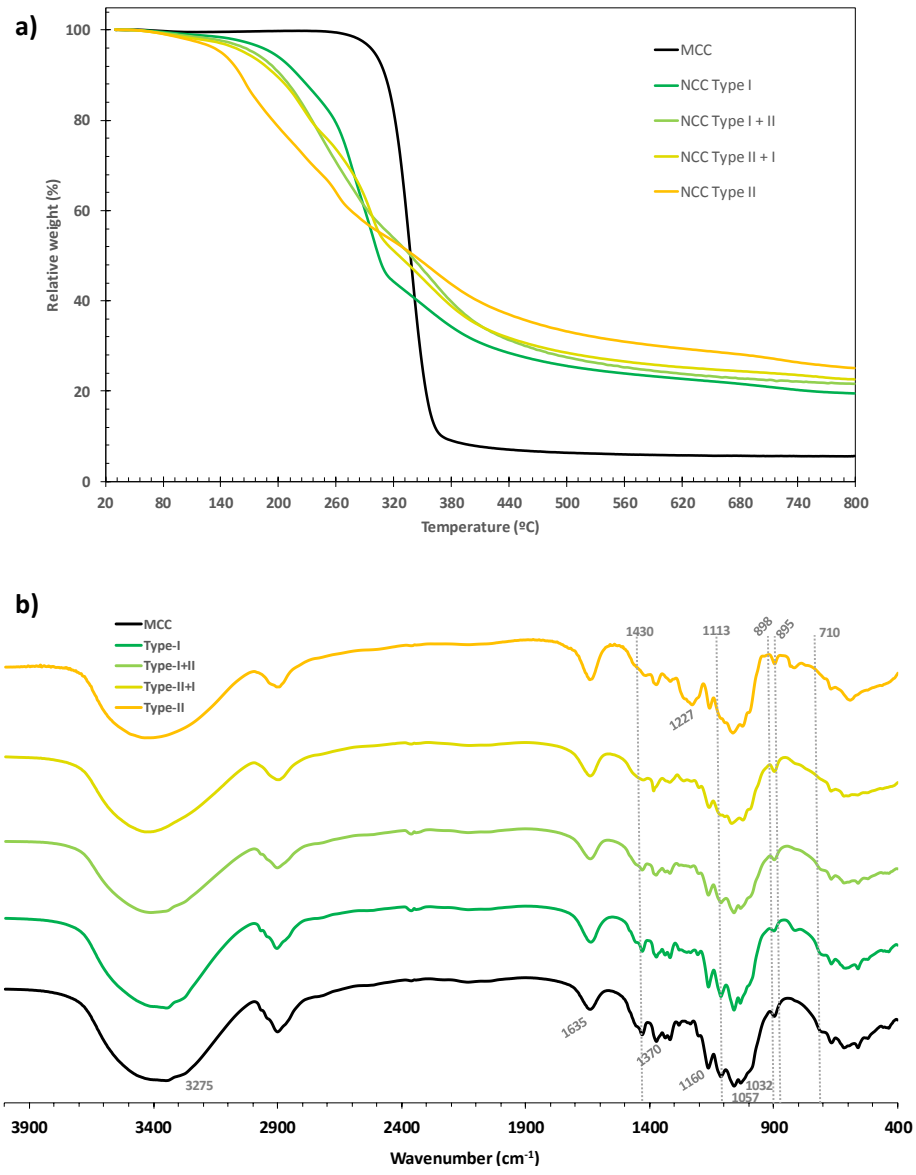

Figure 4.- (a) TGA plots, and (b) FTIR spectra (in %Transmittance) for the different NCC samples and their parent MCC.

SWCNTs dispersions in NCC. Once NCC samples are fully characterized and their synthesis process is understood, we tested them as dispersants for SWCNTs, leading to stable dispersions. We herein demonstrate that the nature of such colloids go far beyond a mere actuation of NCC as a dispersive agent of SWCNTs, since a striking synergy between both elements was noticed after stating the stability in water upon ultracentrifugation at 120,000 rcf, which is unprecedented and exceedingly higher than that observed in the same conditions for both separate components. As a matter of fact, these suspensions have shown an extraordinary stability with time, as they remain unaltered and fully stable yet today since these were prepared (more than a year and a half before, by the time this manuscript is submitted). **Figure 5** displays some characterization data on the ultracentrifuged aqueous supernatants of the SWCNT-NCC system. Visible-NIR spectra (**Figure 5a**) show prominent peaks, corresponding to specific van Hove transitions of metallic (M) and semiconducting (S) SWCNTs, consistent with the same features of these SWCNTs ultracentrifuged with commercial surfactants.[32] The NIR purity index is considered to be one of the most precise ways to assess the purity of a SWCNT sample, since the resonant transitions at a specific wavelength are proportional to the actual SWCNT mass, and distinguishable from any other carbon form. Thus, dividing the baseline-subtracted peak area at a given van Hove transition (preferably the S22 one, here from 850 to 1300 nm) by the whole spectral area in this region, the obtained ratio is proportional to the amount of SWCNTs versus other carbon forms, i.e. the carbonaceous purity of the sample (see ref. 32 for full details on this methodology). Centrifugation yields and NIR purity indexes (**Figure 5b**) for SWCNTs seemed very similar when using each NCC allomorph, meaning that there is not a dependence of the NCC allomorph type in their quantitative dispersant behavior. Nevertheless, the morphologies are actually very different in each situation, as observed by TEM (**Figure 6**). In the case of type-I NCC, SWCNTs are loose with individual NCC particles along their axes, in parallel disposition (**Figure 6a-c**). Indeed, this was also observed by Chauvet et al.[29,46] who proposed that the association between SWCNTs and NCC was in parallel adsorption along the NCC's (200) plane, of higher hydrophobicity. According to this assumption, the stabilization mechanism would be a cooperative action between hydrophobic interactions between

SWCNTs and NCC, and long-range electrostatic forces between cellulose nanocrystals.[46] But this only alludes to type-I NCC, since type-II NCC provides a visibly different scenario (**Figure 6d-f**). We found that SWCNTs dispersed in type-II NCC appeared as heavily wrapped, and trapped within an entangled network. In order to compare the morphology and dimensions of the initial SWCNTs, prior to the dispersion in NCC, additional TEM images are shown in **Figure S3** (Supporting Information). Zeta potential and DLS measurements were also applied to the ultracentrifuged supernatants of SWCNTs dispersed in each NCC type, and the obtained data are shown in **Table 3**. These results correlate with those obtained for the bare NCC aqueous colloids (**Figure 2**), being the SWCNT dispersions with type-II NCC of larger hydrodynamic diameters (~ 4-fold) than with type-I NCC, but overall much lower in numbers. Both cases display a high Zeta potential value, in similar values as their 'naked' NCC counterparts, which accounts for their analogous colloidal stability. It is worth noting that interfacing SWCNTs with NCC should in principle entail a neat increase in hydrodynamic size (given the higher aspect ratio of SWCNTs as compared to NCC), but here we have observed the opposite. The overall apparent sizes are reduced to a factor of ¼ from the NCC to the dispersed SWCNT, a fact that we postulate to point towards an extremely efficient SWCNT debundling and individualization (also hinted by TEM). To the best of our knowledge this is the first time that a type-II NCC is used for dispersing carbon nanostructures, and whilst the effects of both allomorphs are similar in terms of yield and optical purity, there are major differences in the eventual morphology and physicochemical characteristics of both systems.

Table 2. Zeta potential and apparent size (in diameter) for SWCNT-NCC dispersions, together with standard deviations.

SWCNTs-NCC	Zeta Potential (mV)	Apparent diameter (nm)
With type-I	-44 ± 2	58 ± 3
With type-II	-30 ± 2	206 ± 12

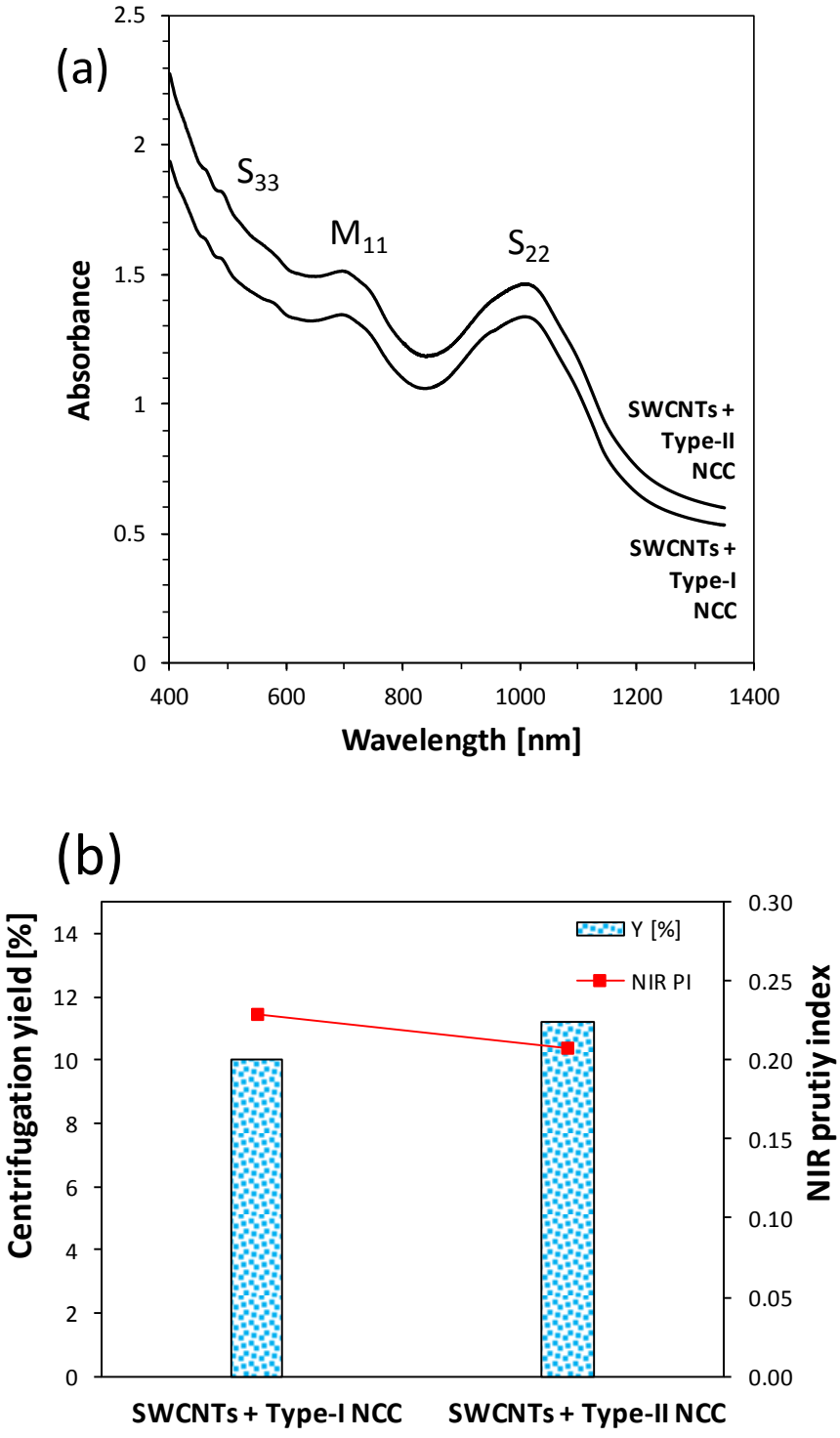

Figure 5.- Characterization data for SWCNTs dispersed in either type-I or type-II NCC (a) Vis-NIR absorbance plots, where van Hove transitions are indicated; (b) centrifugation yields and NIR purity indexes. Mass concentration of SWCNTs in both cases is around 0.1 mg/mL.

Biocompatibility and bioactivity of SWCNT-NCC dispersions. Given the markedly distinct nature of SWCNT hybrids with either type-I or type-II NCC, we investigated whether these hybrids could behave as biocompatible dispersing agents for SWCNTs. In previous reports, we found that SWCNTs induced oxidative stress and altered the normal intestinal function in a rabbit model,[47] even if SWCNTs were purified and wrapped in a hydrophilic dispersant, casting a serious concern on their hypothetical use as a drug vehicle to treat intestinal diseases. However, these adverse effects were mitigated if SWCNTs were purified by dispersion in poly(L-lysine), as tested *in vitro*,[48] thus showing the potential benefits of a proper surface modification of SWCNTs in the design of drug vehicles to treat diseases. In light of the promising behavior of both NCC types to stabilize SWCNTs in water in very different fashions, at this point we focused our scope at ascertaining the effects of such SWCNT-NCC hybrids in the viability of intestinal cells.

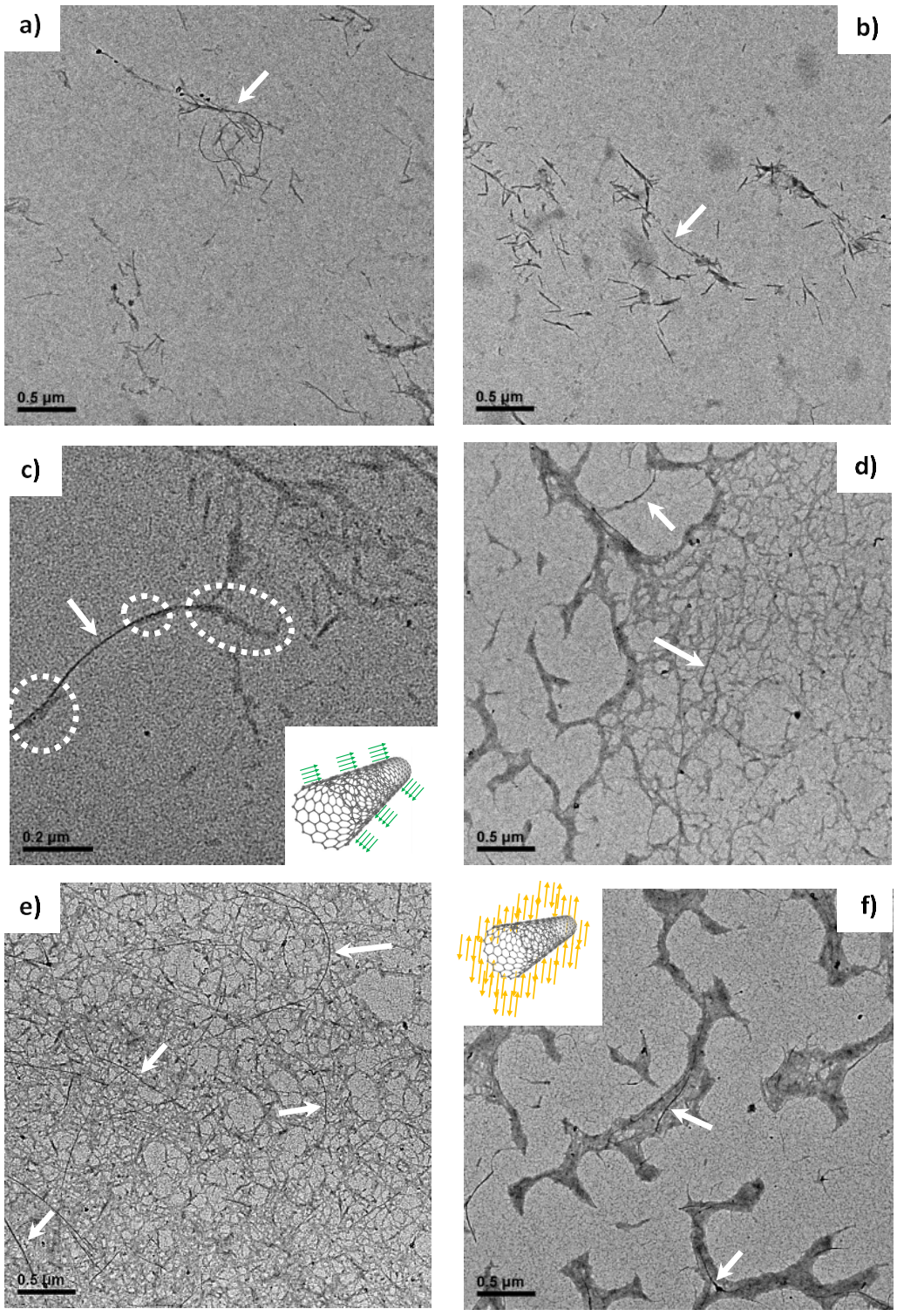

Figure 6.- TEM images of different SWCNT-NCC hybrids. (a-c) with type-I NCC; (d-f) with type-II NCC. Arrows indicate the presence of some SWCNTs while broken-line circles denote the presence of some cellulose nanocrystals. Inset drawings provide a conceptual representation of the SWCNTs dispersed in NCC (same color codes as Scheme 1).

With this purpose, we have run biological studies in Caco-2 human intestinal cells (colon epithelium), through the *in vitro* assessment of cellular viability using the MTT assay, that measures the mitochondrial ability to metabolize MTT by reduction. Viable cells with active metabolism convert MTT into a purple colored formazan product. When cells die, they lose the ability to convert MTT into formazan, thus color formation serves as a useful and convenient marker of only the viable cells. Despite some authors show concern about the reliability of MTT tests in the context of carbon nanostructures, it has been reported that the possible occurrence of undesired effects (such as strong adsorption of chemical species onto SWCNT sidewalls, or insolubilization of formazan crystals) is highly dependent on the employed SWCNT dispersant.[49] In our case, given the strong interaction between SWCNTs and NCC, their stable colloidal state, and the presumed inaccessibility of reaction intermediates to the SWCNTs sidewalls, we assume this test is valid for our viability studies, always bearing in mind these particularities, and disclosing it in a relative manner, comparing among a series of samples of identical nature.

Interestingly, we have used two time points after seeding (5 and 15 days) to obtain cells in different stages of differentiation: undifferentiated cells (5 days) are considered cancer cells and differentiated cells (15 days) are considered normal cells (see experimental section), so we have been able to test two different conditions (normal and cancer) in the same cell line. The obtained results are presented in **Figure 7**. Bare aqueous colloids of NCC were firstly tested, in order to verify their isolated biological effects (**Figure 7a, c, e, g**), and the obtained data illustrate the innocuous nature of NCC, seemingly independent of the allomorph type or the treatment concentration, as cell viability fluctuates close to 100% in all cases. It is worth mentioning that the cytotoxicity and overall biological impact of nanocellulose is still under scrutiny, but there is a major consensus in the fact that single- and low-dose administration of NCC on mammal cells mostly entails a benign behavior.[50] Our results stand in line with this premise, as we did not find any adverse effect in a wide range of concentrations, within the boundaries of what could be considered a non-hazardous and biocompatible material.

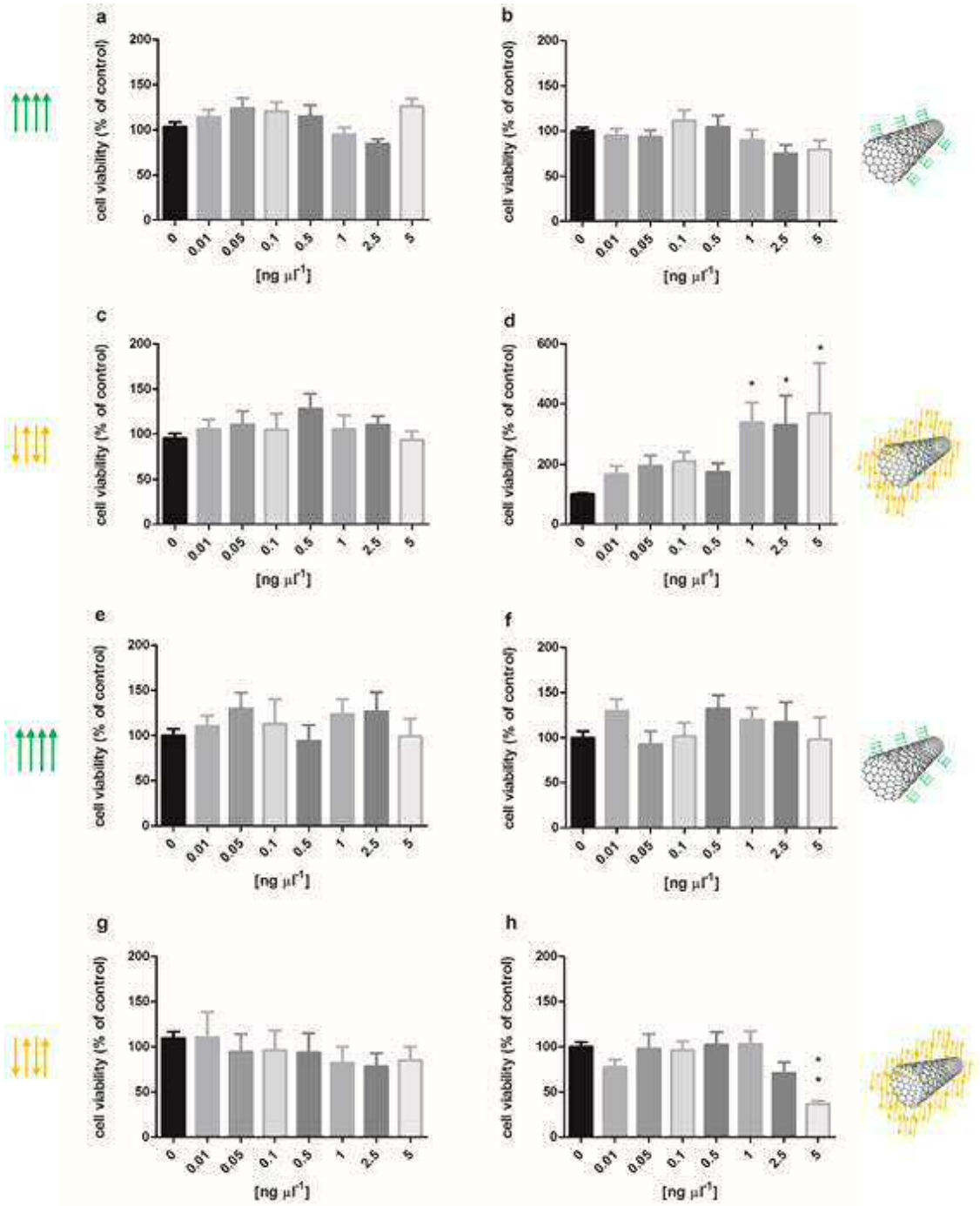

Figure 7.- Graphs showing the viability of normal (15 days after seeding) (a-d) and cancer (5 days after seeding) (e-h) Caco-2 cells treated with NCC and SWCNT-NCC hybrid samples: (a, e) bare NCC type-I; (b, f) SWCNT-NCC(I) hybrid; (c, g) bare NCC type-II; (d, h) SWCNT-NCC(II) hybrid. The results are expressed as mean ± SEM ($n \geq 9$ experiments) *$P<0.05$; **$P<0.01$ vs. control. Visual guideline is provided with the same icons as Scheme 1 and Figure 7 for the representation of NCC and SWNCT-NCC hybrids.

The obtained results for the SWCNT-NCC hybrids (**Figure 7b, d, f, h**), in turn, are quite surprising. While type-I based hybrids display an analogous effect on cell viability as their NCC counterpart, i.e. innocuous towards both kinds of human intestinal cells in the studied concentration range, the type-II based ones show a significantly different behavior. In this latter case, the hybrid displays an even more positive effect towards cancer colon cells at the highest dose tested (5 ng/μL), as it reduces the viability of these cells to about a half, and could be considered a cytotoxic compound for cancer cells and a potential candidate for colon cancer chemotherapy. At the same time, these hybrids increase the mitochondrial metabolism of normal colon cells, improving the cell viability between 200% and 400% in the studied concentration range. We postulate that this unprecedented differential effect of the SWCNT-NCC(II) hybrid on normal and cancer Caco-2 cells, respectively, could be related to its unique morphology, that might trigger different uptake pathways,[51] with a different response depending on the cells' metabolism. The unexpected activation of normal cells' metabolism could be related to this fact, as it might have promoted an enhancement of mitochondrial activity through its own uptake pathway. In any case, a tumorigenic effect is discarded as the explanation for such enhancement, since the cells did not show any abnormal growth pattern during the culture procedure. This dual behavior with no associated drugs or targeting agents might become an innovative colon cancer therapy, favoring the killing of cancer cells while increasing the metabolism of the normal ones. However, further studies will be necessary to fully understand the therapeutic potential of these SWCNT-NCC(II) hybrids (including cellular imaging/tracking techniques and *in vivo* tests) plus the underlying mechanisms leading to this outcome, but as a first insight it looks certainly promising.

CONCLUSION

We have prepared different NCC allomorphs by solely applying sulfuric acid hydrolysis to a biomass source, and the experimental variables (such as the acid concentration, treatment times and temperatures) have been studied in detail in order to tailor the nanocellulose type (from nearly pure type-I to nearly pure type-II, including their mixtures) without the need for mercerization or re-crystallization. Their characterization revealed that such type-II NCC (exclusively coming from acid hydrolysis) presents larger hydrodynamic sizes and sulfate content, leading to unique properties comparted to their mercerized analogues. Taking advantage of the possibility to obtain these NCC allomorphs without adding extra stages to the established acid hydrolysis protocol, this methodology can be considered more affordable and environmentally friendlier. Besides, we have drawn the attention towards the importance and potential of non-mercerized type-II NCC, which is able to provide significant breakthroughs in materials science.

As a proof of principle, we have used these NCCs as SWCNT dispersing agents. Both NCC allomorphs do not only differ in shape and morphology, but behave significantly different, leading to a distinct interaction with SWCNTs enabling enhanced dispersion behavior in aqueous media. Further biological tests of these hybrids with human intestinal (Caco-2) cells reveal that only the one with type-II NCC presents an unprecedented behavior, i.e. simultaneous effect of colon cancer killing and mitochondrial metabolism enhancement of normal cells, while the rest of nanomaterials tested herein display an innocuous trait. To the best of our knowledge, this is the first time a type-II NCC is used as a dispersant for carbon nanotubes, and their resulting dispersion tested in a biomedical application. We showcase the feasibility of reaching a new waterborne hybrid carbon nanomaterial, in a more sustainable and friendlier scheme, possessing great biomedical potential. These preliminary results may pave the way towards the improvement of colon cancer therapies, which is currently under deeper investigation in our laboratories.

ASSOCIATED CONTENT

Supporting Information. Additional thermogravimetric data (differential thermograms and oxygen indexes) of freeze-dried NCC samples. Additional XRD data (peak areas from deconvoluted diffractograms) and more TEM images. This material is available free of charge via the Internet at http://pubs.acs.org.

AUTHOR INFORMATION

Corresponding Author

* jmgonzalez@icb.csic.es (J. M. González-Domínguez).

Author Contributions

The manuscript was written through contributions of all authors. All authors have given approval to the final version of the manuscript. ‡These authors contributed equally.

Funding Sources

This work has received funding from Spanish Ministry of Economy, Industry and Competitiveness (MINEICO) and the Spanish Research Agency (AEI), through GRAPEROS project (Ref. ENE2016-79282-C5-1-R1, and associated EU Regional Development Funds), and a 'Juan de la Cierva – Incorporación' grant (Ref. IJCI-2016-27789). Additional funding from Gobierno de Aragón (Grupo Reconocido DGA T03_17R, A02_17R, and associated EU Regional Development Funds) is acknowledged.

Notes

This work is dedicated to Prof. M. Teresa Martínez.

ACKNOWLEDGMENT

J.M.G.-D. acknowledges Spanish MINEICO for his Juan de la Cierva Incorporación research contract (Ref. IJCI-2016-27789), and E.C. for his PhD fellowship (FPI, Ref. (BES-2017-080020, and associated EU Social Funds).

ABBREVIATIONS

NCC, nanocrystalline cellulose; CNTs, carbon nanotubes; SWCNTs, single-walled carbon nanotubes; MTT (3-(4,5-dimethylthiazol-2-yl)-2,5-diphenyltetrazolium bromide)

REFERENCES

[1] Shchipunov, Y. Bionanocomposites: Green Sustainable Materials for the near Future. *Pure Appl. Chem.* **2012**, *84*, 2579–2607.

[2] Abitbol, T.; Rivkin, A.; Cao, Y.; Nevo, Y.; Abraham, E.; Ben-Shalom, T.; Lapidot, S.; Shoseyov, O. Nanocellulose, a Tiny Fiber with Huge Applications. *Curr. Opin. Biotechnol.* **2016**, *39*, 76–88.

[3] Kargarzadeh, H.; Mariano, M.; Gopakumar, D.; Ahmad, I.; Thomas, S.; Dufresne, A.; Huang, J.; Lin, N. Advances in Cellulose Nanomaterials. *Cellulose* **2018**, *25*, 2151-2189.

[4] Dufresne, A. Nanocellulose: A New Ageless Bionanomaterial. *Mater. Today* **2013**, *16* (6), 220–227.

[5] Grishkewich, N.; Mohammed, N.; Tang, J.; Tam, K. C. Recent Advances in the Application of Cellulose Nanocrystals. *Curr. Opin. Colloid Interface Sci.* **2017**, *29*, 32–45.

[6] Ummartyotin, S.; Manuspiya, H. A Critical Review on Cellulose: From Fundamental to an Approach on Sensor Technology. *Renew. Sustain. Energy Rev.* **2015**, *41*, 402–412.

[7] Kim, N. H.; Imai, T.; Wada, M.; Sugiyama, J. Molecular Directionality in Cellulose Polymorphs. *Biomacromolecules* **2006**, *7*, 274–280.

[8] Gong, J.; Mo, L.; Li, J. A Comparative Study on the Preparation and Characterization of Cellulose Nanocrystals with Various Polymorphs. *Carbohydr. Polym.* **2018**, *195*, 18–28.

[9] Ko, S. W.; Soriano, J. P. E.; Rajan Unnithan, A.; Lee, J. Y.; Park, C. H.; Kim, C. S. Development of Bioactive Cellulose Nanocrystals Derived from Dominant Cellulose Polymorphs I and II from Capsosiphon Fulvescens for Biomedical Applications. *Int. J. Biol. Macromol.* **2018**, *110*, 531–539.

[10] Pinkert, A.; Marsh, K. N.; Pang, S. Reflections on the Solubility of Cellulose. *Ind. Eng. Chem. Res.* **2010**, *49*, 11121–11130.

[11] Liu, Z.; Sun, X.; Hao, M.; Huang, C.; Xue, Z.; Mu, T. Preparation and Characterization of Regenerated Cellulose from Ionic Liquid Using Different Methods. *Carbohydr. Polym.* **2015**, *117*, 54–62.

[12] Ciolacu, D.; Ciolacu, F.; Popa, V. I. Amorphous Cellulose – Structure and Characterization. *Cellulose Chem. Technol.* **2011**, *45*, 13–21.

[13] Ferguson, A.; Khan, U.; Walsh, M.; Lee, K.; Bismarck, A.; Shaffer, M. S. P.; Coleman, J. N.; Bergin, S. D. Understanding the Dispersion and Assembly of Bacterial Cellulose in Organic Solvents. *Biomacromolecules* **2016**, *17*, 1845–1853.

[14] Sèbe, G.; Ham-Pichavant, F.; Ibarboure, E.; Koffi, A. L. C.; Tingaut, P. Supramolecular Structure Characterization of Cellulose II Nanowhiskers Produced by Acid Hydrolysis of Cellulose I Substrates. *Biomacromolecules* **2012**, *13*, 570–578.

[15] Khili, F.; Borges, J.; Almeida, P. L.; Boukherroub, R.; Omrani, A. D. Extraction of Cellulose Nanocrystals with Structure I and II and Their Applications for Reduction of Graphene Oxide and Nanocomposite Elaboration. *Waste Biomass Valoriz.* **2018**, *0*, 1–15.

[16] Merlini, A.; Souza, V. C. D. E.; Gomes, R. M.; Coirolo, A.; Machado, R. A. F.; Merlini, A. Effects of reaction conditions on the shape and crystalline structure of cellulose nanocrystals. *Cellulose Chem. Technol.* **2018**, *52*, 325–335.

[17] Xing, L.; Gu, J.; Zhang, W.; Tu, D.; Hu, C. Cellulose I and II Nanocrystals Produced by Sulfuric Acid Hydrolysis of Tetra Pak Cellulose I. *Carbohydr. Polym.* **2018**, *192*, 184–192.

[18] Flauzino Neto, W. P.; Putaux, J. L.; Mariano, M.; Ogawa, Y.; Otaguro, H.; Pasquini, D.; Dufresne, A. Comprehensive Morphological and Structural Investigation of Cellulose I and II Nanocrystals Prepared by Sulphuric Acid Hydrolysis. *RSC Adv.* **2016**, *6*, 76017–76027.

[19] Li, X.; Li, J.; Gong, J.; Kuang, Y.; Mo, L.; Song, T. Cellulose Nanocrystals (CNCs) with Different Crystalline Allomorph for Oil in Water Pickering Emulsions. *Carbohydr. Polym.* **2018**, *183*, 303–310.

[20] Chundawat, S. P. S.; Bellesia, G.; Uppugundla, N.; Da Costa Sousa, L.; Gao, D.; Cheh, A. M.; Agarwal, U. P.; Bianchetti, C. M.; Phillips, G. N.; Langan, P.; Balan, V.; Gnanakaran, S.; Dale, B. E. Restructuring the Crystalline Cellulose Hydrogen Bond Network Enhances Its Depolymerization Rate. *J. Am. Chem. Soc.* **2011**, *133*, 11163–11174.

[21] Wada, M.; Ike, M.; Tokuyasu, K. Enzymatic Hydrolysis of Cellulose I Is Greatly Accelerated via Its Conversion to the Cellulose II Hydrate Form. *Polym. Degrad. Stab.* **2010**, *95*, 543–548.

[22] Ling, Z.; Zhang, X.; Yang, G.; Takabe, K.; Xu, F. Nanocrystals of Cellulose Allomorphs Have Different Adsorption of Cellulase and Subsequent Degradation. *Ind. Crops Prod.* **2018**, *112*, 541–549.

[23] Chauhan, P. S. in *Hybrid Nanomaterials: Synthesis, Characterization, and Applications*, **2011**, Ed. John Wiley & sons, DOI: 10.1002/9781118003497.

[24] Skaltsas, T.; Stergiou, A.; Chronopoulos, D. D.; Zhao, S.; Shinohara, H.; Tagmatarchis, N. All-Carbon Nanosized Hybrid Materials: Fluorescent Carbon Dots Conjugated to Multiwalled Carbon Nanotubes. *J. Phys. Chem. C* **2016**, *120*, 8550-8558.

[25] Chen, C.; Zhang, T.; Zhang, Q.; Chen, X.; Zhu, C.; Xu, Y.; Yang, J.; Liu, J.; Sun, D. Biointerface by Cell Growth on Graphene Oxide Doped Bacterial Cellulose/Poly(3,4-ethylenedioxythiophene) Nanofibers. *ACS Appl. Mater. Interfaces* **2016**, *8*, 10183-10192.

[26] Hamedi, M. M.; Hajian, A.; Fall, A. B.; Hakanson, K.; Salajkova, M.; Lundell, F.; Wagberg, L.; Berglund, L. A. Highly conducting, strong nanocomposites based on nanocellulose-assisted aqueous dispersions of single-wall carbon nanotubes. *ACS Nano* **2014**, *8*, 2467-2476.

[27] Li, Y.; Zhu, H.; Wang, Y.; Ray, U.; Zhu, S.; Dai, J.; Chen, C.; Fu, K.; Jang, S.-H.; Henderson, D.; Li, T.; Hu, L. Cellulose-Nanofiber-Enabled 3D Printing of a Carbon-Nanotube Microfiber Network. *Small Methods* **2017**, *1*, 1700222.

[28] Hajian, A.; Lindström, S. B.; Pettersson, T.; Hamedi, M. H.; Wagberg, L. Understanding the Dispersive Action of Nanocellulose for Carbon Nanomaterials. *Nano Lett.* **2017**, *17*, 1439-1447.

[29] Mougel, J.-B.; Adda, C.; Bertoncini, P.; Capron, I.; Cathala, B.; Chauvet, O. Highly efficient and predictable noncovalent dispersion of single-walled and multi-walled carbon nanotubes by cellulose nanocrystals. *J. Phys. Chem. C* **2016**, *120*, 22694-22701.

[30] González-Domínguez, J. M.; León, V.; Lucío, M. I.; Prato, M.; Vázquez, E. Production of Ready-to-Use Few-Layer Graphene in Aqueous Suspensions. *Nat. Protoc.* **2018**, *13* (3), 495–506.

[31] González-Domínguez, J. M.; Neri, W.; Maugey, M.; Poulin, P.; Ansón-Casaos, A.; Martínez, M. T. A chemically reactive spinning dope for significant improvements in wet spun carbon nanotube fibres. *Chem. Commun.* **2013**, *49*, 3973-3975.

[32] Ansón-Casaos, A.; González-Domínguez, J. M.; Lafragüeta, I.; Carrodeguas, J. A.; Martínez, M. T. Optical Absorption Response of Chemically Modified Single-Walled Carbon Nanotubes upon Ultracentrifugation in Various Dispersants. *Carbon* **2014**, *66*, 105–118.

[33] Mesonero, J.; Mahraoui, L.; Matosin, M.; Rodolosse, A.; Rousset, M.; Brot-Laroche, E., Expression of the hexose transporters GLUT1-GLUT5 and SGLT1 in clones of Caco-2 cells. *Biochem. Soc. Trans.* **1994,** *22* (3), 681-4.

[34] Zucco, F.; Batto, A. F.; Bises, G.; Chambaz, J.; Chiusolo, A.; Consalvo, R.; Cross, H.; Dal Negro, G.; de Angelis, I.; Fabre, G.; Guillou, F.; Hoffman, S.; Laplanche, L.; Morel, E.; Pincon-Raymond, M.; Prieto, P.; Turco, L.; Ranaldi, G.; Rousset, M.; Sambuy, Y.; Scarino, M. L.; Torreilles, F.; Stammati, A., An inter-laboratory study to evaluate the effects of medium composition on the differentiation and barrier function of Caco-2 cell lines. *Altern. Lab Anim.* **2005**, 33 (6), 603-18.

[35] Camacho, F.; González-Tello, P.; Jurado, E.; Robles, A. Microcrystalline-Cellulose Hydrolysis with Concentrated Sulphuric Acid. *J. Chem. Technol. Biotechnol.* **1996**, *67* (4), 350–356.

[36] Ioelovich, M. Study of Cellulose Interaction with Concentrated Solutions of Sulfuric Acid. *ISRN Chem. Eng.* **2012**, *2012*, 1–7.

[37] Park, S.; Baker, J. O.; Himmel, M. E.; Parilla, P. A.; Johnson, D. K. Cellulose Crystallinity Index: Measurement Techniques and Their Impact on Interpreting Cellulase Performance. *Biotechnol. Biofuels* **2010**, *3* (1), 10.

[38] Daicho, K.; Saito, T.; Fujisawa, S.; Isogai, A. The Crystallinity of Nanocellulose: Dispersion-Induced Disordering of the Grain Boundary in Biologically Structured Cellulose. *ACS Appl. Nano Mater.* **2018**, *1* (10), 5774–5785.

[39] Lu, P.; Hsieh, Y. Lo. Preparation and Properties of Cellulose Nanocrystals: Rods, Spheres, and Network. *Carbohydr. Polym.* **2010**, *82* (2), 329–336.

[40] Lin, N.; Dufresne, A. Surface Chemistry, Morphological Analysis and Properties of Cellulose Nanocrystals with Gradiented Sulfation Degrees. *Nanoscale* **2014**, *6* (10), 5384–5393.

[41] Gupta, P. K.; Uniyal, V.; Naithani, S. Polymorphic Transformation of Cellulose i to Cellulose II by Alkali Pretreatment and Urea as an Additive. *Carbohydr. Polym.* **2013**, *94* (2), 843–849.

[42] Foster, E. J.; Moon, R. J.; Agarwal, U. P.; Bortner, M. J.; Bras, J.; Camarero-Espinosa, S.; Chan, K. J.; Clift, M. J. D.; Cranston, E. D.; Eichhorn, S. J.; Fox, D. M.; Hamad, W. Y.; Heux, L.; Jean, B.; Matthew, K.; Nieh, W.; Ong, K. J.; Reid, M. S.; Renneckar, S.; Roberts, R.; Shatkin, J. A.; Simonsen, J.; Stinson-Bagby, K.; Wanasekara, N.; Youngblood, J. Current Characterization Methods for Cellulose Nanomaterials. *Chem. Soc. Rev.* **2018**, 47 (8), 2609–2679.

[43] Lichtenstein, K.; Lavoine, N. Toward a Deeper Understanding of the Thermal Degradation Mechanism of Nanocellulose. *Polym. Degrad. Stab.* **2017**, 146, 53–60.

[44] González-Domínguez, J. M.; Ansón-Casaos, A.; Castell, P.; Díez-Pascual, A. M.; Naffakh, M.; Ellis, G.; Gómez, M. A.; Teresa Martínez, M. Integration of Block Copolymer-Wrapped Single-Wall Carbon

Nanotubes into a Trifunctional Epoxy Resin. Influence on Thermal Performance. *Polym. Degrad. Stab.* **2010**, 95 (10), 2065–2075.

[45] O'Sullivan, A. C. Cellulose: The Structure Slowly Unravels. *Cellulose* **1997**, 4, 173-207.

[46] Olivier, C.; Moreau, C.; Bertoncini, P.; Bizot, H.; Chauvet, O.; Cathala, B. Cellulose Nanocrystal-Assisted Dispersion of Luminescent Single-Walled Carbon Nanotubes for Layer-by-Layer Assembled Hybrid Thin Films. *Langmuir* **2012**, *28* (34), 12463–12471.

[47] Grasa, L.; Ansón-Casaos, A.; Martínez, M. T.; Albendea, R.; De Martino, A.; Gonzalo, S.; Murillo, M. D. Single-Walled Carbon Nanotubes (SWCNTs) Enhance KCl-, Acetylcholine-, and Serotonin-Induced Contractions and Evoke Oxidative Stress on Rabbit Ileum. *J. Biomed. Nanotechnol.* **2014**, *10* (3), 529–542.

[48] Ansón-Casaos, A.; Grasa, L.; Pereboom, D.; Mesonero, J. E.; Casanova, A.; Murillo, M. D.; Martínez, M. T. In-Vitro Toxicity of Carbon Nanotube/Polylysine Colloids to Colon Cancer Cells. *IET Nanobiotechnology* **2016**, *10* (6), 374–381.

[49] Belyanskaya, L.; Manser, P.; Spohn, P.; Bruinink, A.; Wick, P. The Reliability and Limits of the MTT Reduction Assay for Carbon Nanotubes-Cell Interaction. *Carbon* **2007**, *45* (13), 2643–2648.

[50] Endes, C.; Camarero-Espinosa, S.; Mueller, S.; Foster, E. J.; Petri-Fink, A.; Rothen-Rutishauser, B.; Weder, C.; Clift, M. J. D. A Critical Review of the Current Knowledge Regarding the Biological Impact of Nanocellulose. *J. Nanobiotechnology* **2016**, *14* (1), 78.

[51] Song, S.; Fu, H.; He, B.; Wang, D.; Qin, M.; Yang, D.; Liu, D.; Song, G.; Shi, Y.; Zhang, H.; Wang, X.; Dai, W.; Zhang, Q. Rho GTPases in A549 and Caco-2 Cells Dominating the Endocytic Pathways of Nanocarbons with Different Morphologies. *Int. J. Nanomedicine* **2018**, *13*, 4391–4404.

TOC GRAPHIC

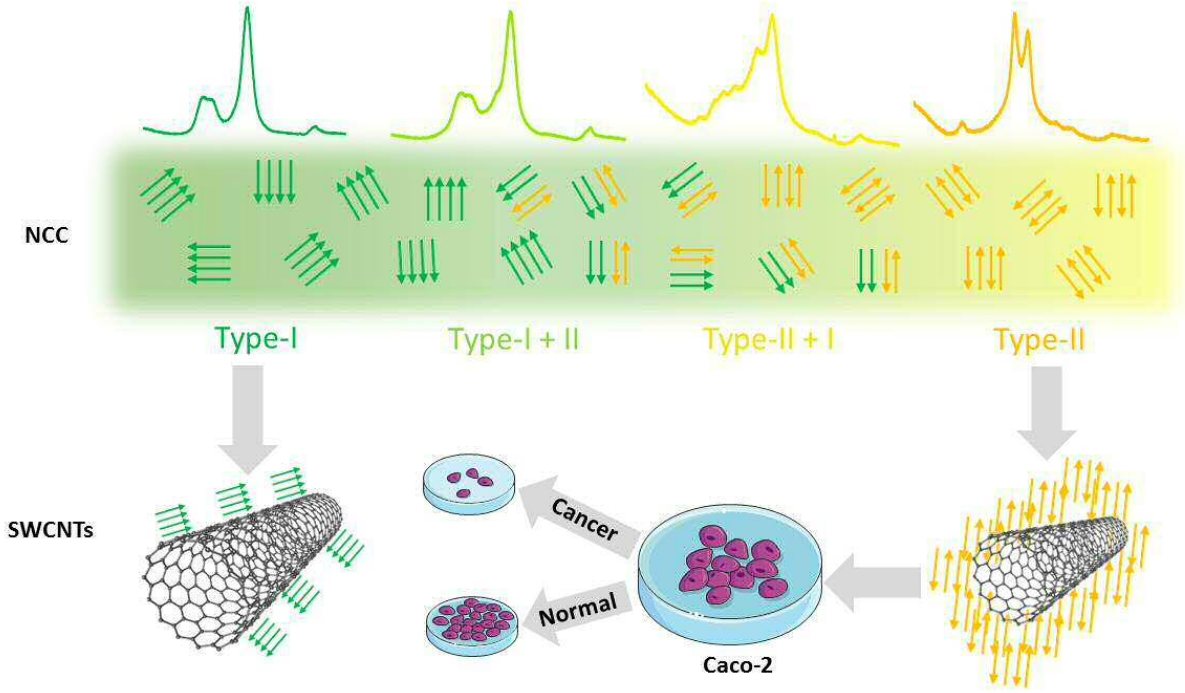
NCC
Type-I
Type-I + II
Type-II + I
Type-II
SWCNTs
Cancer
Normal
Caco-2